Deep Space Wide Area Search Strategies

Michael Capps
Colorado State University
1st Lt Julian McCafferty
Air Force Maui Optical & Supercomputing Site (AMOS)

Abstract

There is an urgent need to expand the space situational awareness (SSA) mission beyond catalog maintenance to providing near real-time indications and warnings of emerging events. While building and maintaining a catalog of space objects is essential to SSA, this does not address the threat of uncatalogued and uncorrelated deep space objects. The Air Force therefore has an interest in transformative technologies to scan the geostationary (GEO) belt for uncorrelated space objects. Traditional ground based electro-optical sensors are challenged in simultaneously detecting dim objects while covering large areas of the sky using current CCD technology. Time delayed integration (TDI) scanning has the potential to enable significantly larger coverage rates while maintaining sensitivity for detecting near-GEO objects. This paper investigates strategies of employing TDI sensing technology from a ground based electro-optical telescope, toward providing tactical indications and warnings of deep space threats. We present results of a notional wide area search TDI sensor that scans the GEO belt from three locations: Maui, New Mexico, and Diego Garcia. Deep space objects in the NASA 2030 debris catalog are propagated over multiple nights as an indicative data set to emulate notional uncatalogued near-GEO orbits which may be encountered by the TDI sensor. Multiple scan patterns are designed and simulated, to compare and contrast performance based on 1) efficiency in coverage, 2) number of objects detected, and 3) rate at which detections occur, to enable follow-up observations by other space surveillance network (SSN) sensors. A step-stare approach is also modeled using a dedicated, co-located sensor notionally similar to the Ground-Based Electro-Optical Deep Space Surveillance (GEODSS) tower. Equivalent sensitivities are assumed. This analysis quantifies the relative benefit of TDI scanning for the wide area search mission.

Background

A representative model of a single Ground Based-Electro-Optical Deep Space Surveillance (GEODSS) telescope tower is generated as a baseline for comparing horizontal and vertical search patterns using a step-and-stare and TDI type search. The GEODSS system consists of three sites in Hawaii, New Mexico, and Diego Garcia, each consisting of three identical telescopes on equatorial mounts [1]. This mount is well suited for equatorial type searches by stepping the telescope FOV along the declination (latitude) and right ascension (longitude). This step-and-stare equatorial search will henceforth be referred to as the "Fast Search". The current GEODSS sensors consisting of an array of 1960 by 2560 pixels and produce a 1.23 x 1.61 degree rectangular field of view (FOV) [1]. The GEODSS camera FOV and CCD geometry are used for the sensor model; however, all other sensor parameters are notional such that the simulation results are relative and do not represent the operational performance of its current configuration.

The notional TDI type sensor is modeled in this simulation using the same CCD geometry and sensor FOV as the current GEODSS telescope; however, the readout of the camera would instead be by pixel row at the scan rate of the telescope. The 1.61 degree side of the rectangular FOV is used as the single direction scanning face of the modeled TDI sensor. Time delayed integration (TDI) scanning consists of moving the sensor continuously (relative to a stationary object being imaged) and delaying integration by moving partial measurements to neighboring rows of photosensitive elements. TDI sensing has the potential to enable significantly larger coverage rates than more traditional step-and-stare searches while maintaining sensitivity for detecting near-geo objects. While TDI has been used for many years in other applications, there has been little research in the application of TDI for large sky surveys to support SSA. This research aims to quantify the predicted performance of various TDI search strategies relative to the conventional GEODSS Fast Search approach.

Procedure

A simulation is built which propagates objects from the NASA 2030 simulated debris catalog made up of 176,228 TLEs. Because this study focuses on near-geo objects, the catalog is restricted to objects with eccentricity less than 0.01 (near-circular), inclination of less than 20 degrees, and mean motion between 0.99 and 1.01. This set of objects is propagated through 10 nights from the 1 January 2030 orbit epoch to 10 January 2030. To account for any bias in the start time of the search, the simulation includes three different start times: sunset, several hours after sunset, and such that the search ends at sunrise. Two categories of search patterns are simulated, vertical and horizontal searches, each with four variations based on which corner of the search area they begin: Northeast, Southeast, Northwest, and Southwest. Vertical search patterns scan up or down lines of longitude while horizontal search patterns scan along lines of latitude. It is assumed for each search that the TDI sensor can only scan in a single direction, and that the mount is mechanically incapable of rotating 180 degrees in the polar axis, requiring each pass of the TDI search to start and end on the same side. A 0.1 degree overlap is used between each scan and FOV. The search area, or FOR (Field of Regard), is bounded by +/- 45 degrees in longitude from local zenith at each site and +/- 20 degrees in latitude, projected out from the Earth to 35,786 km. This captures the vast majority of near-geosynchronous objects available to a given ground site.

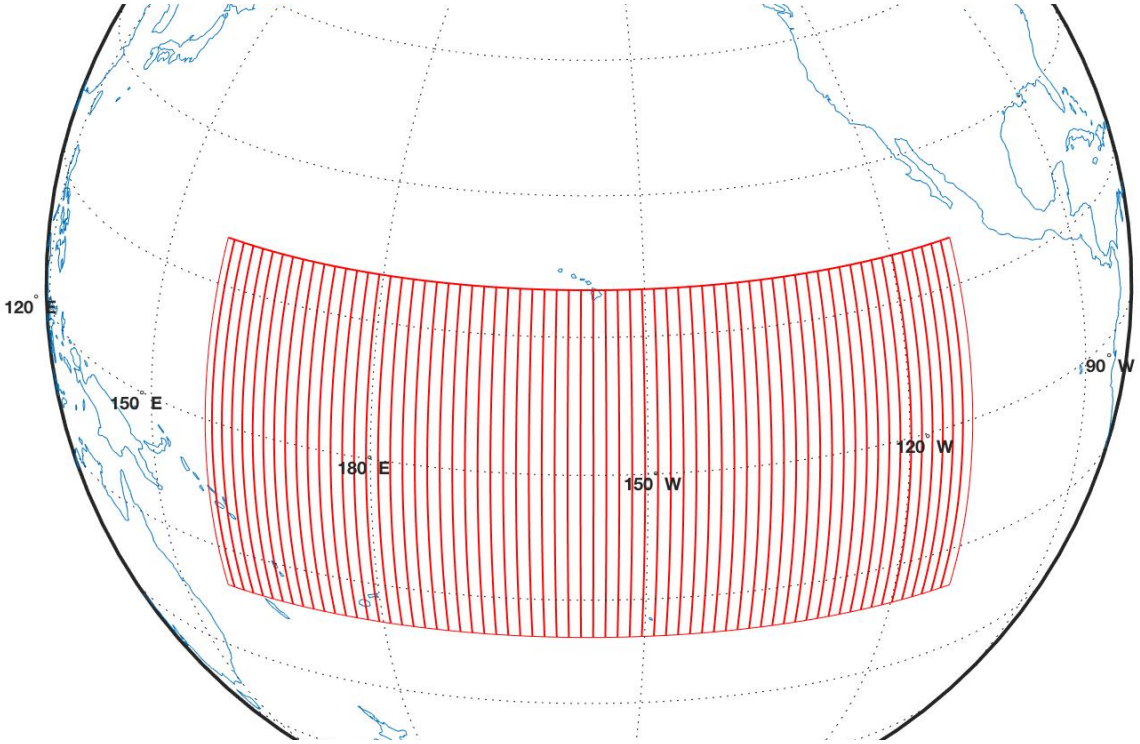

Figure 1: Maui search area projected onto the Earth

Perhaps the most important tradeoff when designing a wide area search is between the coverage rate and limiting detectable visual magnitude. This relationship is dependent both on the sensitivity of the camera in maximizing the SNR, and the astrometric processing to detect the lowest possible SNR. Additional details for determining an optical system's limiting magnitude and SNR can be found in Reference 2. The signal captured from any given detection can be determined from Equation 1 where A_t is the cross-sectional area of the target, ρ is the target albedo, Δt is the integration time, R is the distance from the target to the sensor, f_Ψ is the phase angle factor, E_{sun} is the total flux from the sun in the spectral range of the system, and T_{sys} is the system throughput. All objects from the NASA Debris Catalog

are treated as Lambertian Spheres with a phase angle factor shown in Equation 2. The system throughput is dependent on the sensor and environment as shown in Equation 3 where A_{sensor} is the acquisition area of the telescope, τ_{atm} is the atmospheric extinction factor, τ_{opt} is the optical transmission factor, QE is the camera Quantum Efficiency, and $\frac{\lambda}{hc}$ serves as the conversion from Watts to photons per second.

$$n_{signal} = \frac{A_t \rho \Delta t}{R^2} f_\Psi \sum_{\lambda=350}^{1100} E_{sun}\, T_{sys} \quad \text{Eq 1}$$

$$f_\Psi = \frac{2}{3\pi^2}[sin\Psi + (\pi - \Psi)cos\Psi] \quad \text{Eq 2}$$

$$T_{sys} = A_{sensor} \tau_{\mathrm{atm}} \tau_{opt} QE \frac{\lambda}{hc} \quad \text{Eq 3}$$

The system noise is also largely driven by the sensor performance as shown in Equation 4 and Equation 5 where τ_{blur} is the camera blur efficiency, $n_{celestial\ noise}$ is the celestial background noise, n_{dark} is the dark current noise, n_{read} is the read noise, and n_q is the quantization noise.

$$n_{noise} = \sqrt{\tau_{blur} n_{signal} + \Delta t (n_{celestial\ noise}^2 + n_{dark}^2) + n_{CCD}^2} \quad \text{Eq 4}$$

$$n_{CCD} = Binning \sqrt{n_{read}^2 + n_q} \quad \text{Eq 5}$$

Finally, the apparent visual magnitude of any given target is determined by Equation 6. The limiting detectable magnitude can be calculated by solving the SNR equation for the integration time given a threshold SNR for detection and its corresponding flux.

$$m_a - m_b = -2.5 \log_{10}\left(\frac{f_a}{f_b}\right) \quad \text{Eq 6}$$

It is important to note that this study does not quantify the performance of the GEODSS system but rather the relative performance of a traditional Fast Search and a TDI scan using the GEODSS sensor geometry and notional camera specifications. A number of assumptions about the camera performance and atmospheric conditions are necessary but remain consistent between the two models. Detecting dim space objects among a celestial background is a science in itself, and outside of the scope of this study; therefore, it is assumed a minimum SNR of 6 can be detected through image processing. Coverage rate is also bounded by user defined and mechanically set limits of the telescope mount to accelerate, slew, and settle between exposures. A simplifying assumption of a 2 deg/sec slew rate is used to account for acceleration and settle times for all search patterns between exposures. The relationship between the limiting detectable visual magnitude and coverage rate using the preceding assumptions is presented for the two sensors in Figure 2. A coverage rate of 1000 deg^2 per hour is fixed for all results presented in this study, leaving the limiting magnitude variable for each search.

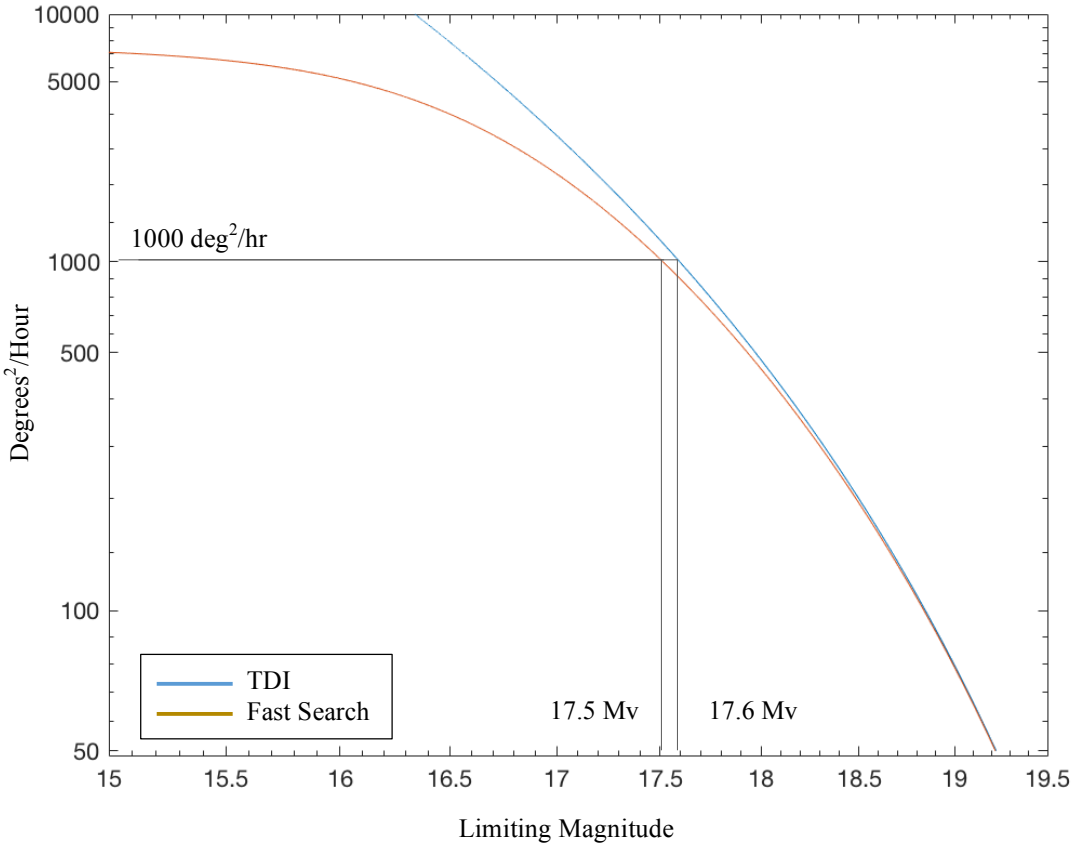

Figure 2: Coverage rate vs limiting magnitude for a Geostationary object

Results and Analysis

The two primary performance metrics used to compare the various search patterns are the number of objects which cross the telescope FOV and the number of objects detected relative to the total number of objects in the FOR. The number of detections is determined by the total number of objects that cross the FOV with an SNR threshold above 6 using the calculations detailed in the Procedure and cross-sectional area provided in the NASA 2030 Debris Catalog. The following tables display the results for each ground site across 10 nights of operations.

Table 1: Search pattern detection results for 1000 deg^2/sec coverage rate across 10 nights in Maui

	Total Objects in FOR	**Total Objects that Cross FOV**	**Total Detections**
Vertical Search TDI	13315	13021	9030
Horizontal Search TDI	13315	11507	7596
Vertical Fast Search	13315	12986	8661
Horizontal Fast Search	13315	11243	7061

Table 2: Search pattern detection results for 1000 deg^2/sec coverage rate across 10 nights in New Mexico

	Total Objects in FOR	**Total Objects that Cross FOV**	**Total Detections**
Vertical Search TDI	13281	12779	8830
Horizontal Search TDI	13281	11374	7573
Vertical Fast Search	13281	12768	8710
Horizontal Fast Search	13281	10893	7075

Table 3: Search pattern detection results for 1000 deg^2/sec coverage rate across 10 nights in Diego Garcia

	Total Objects in FOR	Total Objects that Cross FOV	Total Detections
Vertical Search TDI	10648	10330	8332
Horizontal Search TDI	10648	9547	7223
Vertical Fast Search	10648	10329	7935
Horizontal Fast Search	10648	9309	6672

Detection results between the TDI and Fast Searches for a 1000 deg^2/sec coverage rate demonstrate a 2.5% increase in detections averaged across the ground sites for vertical TDI searches, and a 2.9% increase in detections averaged across the ground sites for horizontal TDI searches. Even though the search patterns perform slightly differently depending on the date (varying between 96% and 99% objects seen), when averaged over all dates and locations, approximately 97% of objects cross the FOV in the vertical search patterns while 86% of objects cross the FOV during horizontal search patterns. This difference between horizontal and vertical patterns is a result of higher inclination objects transiting more quickly between North and South near the equator. Increasing the amount of overlap between neighboring scans across the region or decreasing the coverage rate can reduce or eliminate these missed targets. Uncontrolled geostationary orbits tend to drift in inclination at an initial rate of approximately 0.8° per year up to ~15° due to third body gravitational forces from the sun and moon and the Earth's oblateness [4]. This well understood phenomenon is reflected in geo debris prediction models including the NASA 2030 Debris Catalog used in this simulation, so it is well known that the debris population in these high inclination geosynchronous orbits will be increasing in the coming years.

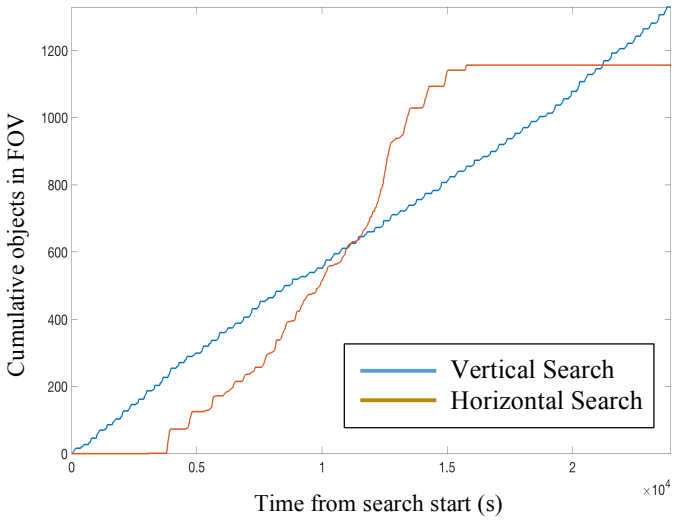

Figure 3: Cumulative objects in FOV for Maui Fast Search

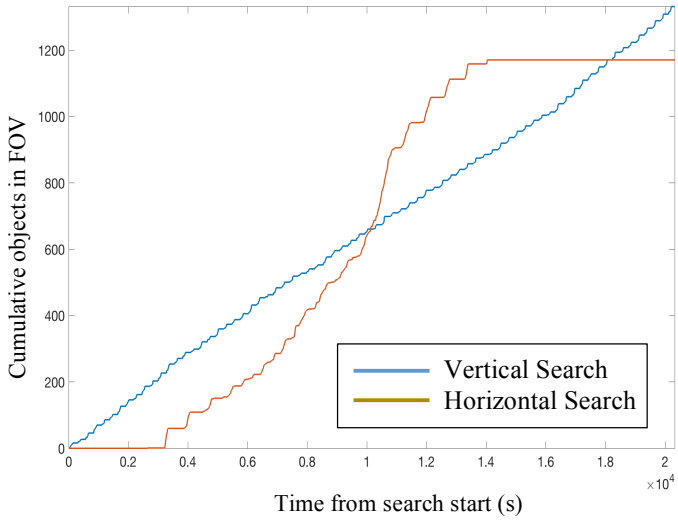

Figure 4: Cumulative objects in FOV for Maui TDI Search

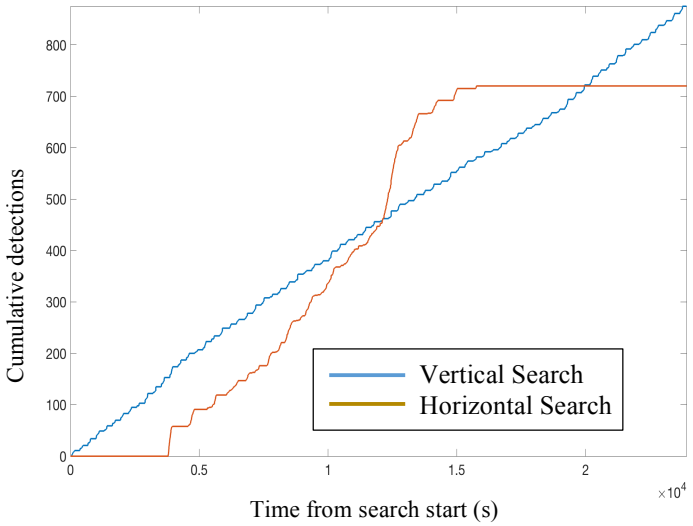

Figure 5: Cumulative objects detected for Maui Fast Search

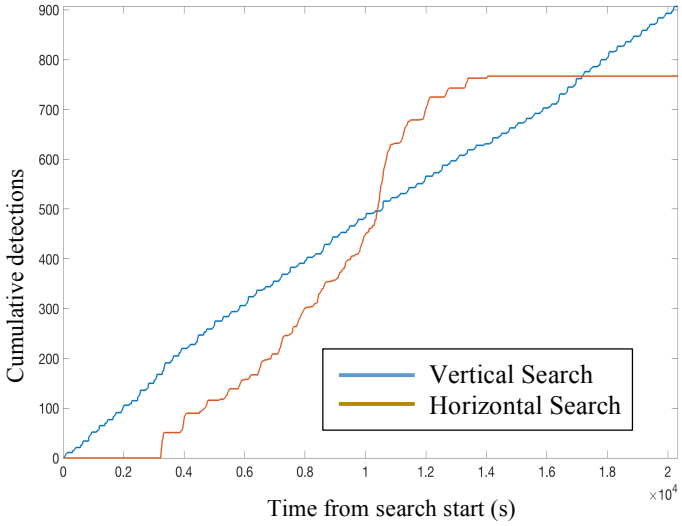

Figure 6: Cumulative objects detected for Maui TDI Search

While the 2030 debris catalog includes predicted high inclination geosynchronous debris, the high inclination region (above 10°) is still relatively sparse as reflected in the horizontal search results. As expected, the density of deep space objects near the geostationary belt is extremely high, resulting in the vast majority of detections occurring in geostationary region for the horizontal search, whereas the vertical search has a near linear spread of detections throughout the search. Note that these figures do not include revisits of objects already seen during a search. The horizontal searches include a greater number of revisits than the vertical searches, so the impact of these additional views exaggerates the difference between the two search patterns. Results for New Mexico and Diego Garcia are largely similar and thus not presented here.

Two additional performance metrics are the rate of detections and rate at which objects cross the FOV. The rates are measured by summing the total number of detections or objects that cross the FOV during the previous 5 minutes of the simulation. This metric is significant for initial orbit determination (IOD) of uncorrelated tracks (UCTs). Angles-only IOD of near-geosynchronous objects with electro-optical sensors has been shown to require a follow-up observation within 5 minutes of initial detection, otherwise additional observations cannot be associated with high confidence [3]. Using the NASA 2030 Debris Catalog as a data set, this detection rate provides a representative running window of potential UCTs which may require a follow-up observation to build an orbit before the candidate orbit expires.

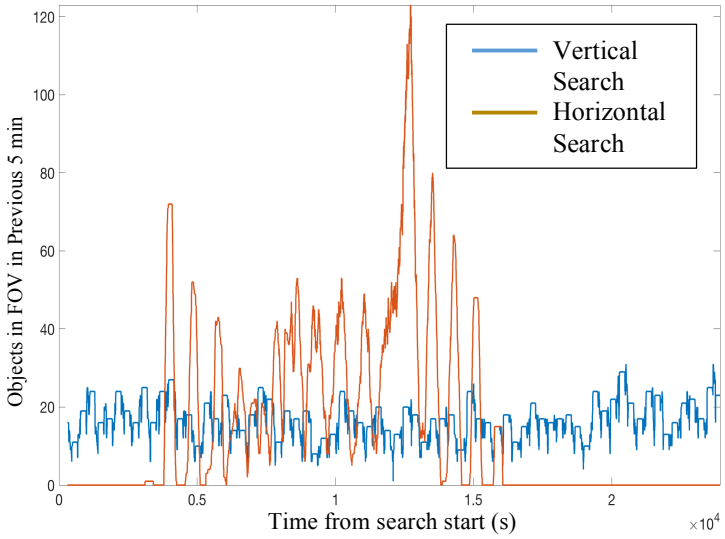

Figure 7: Objects in FOV in previous 5 min for Maui Fast Search

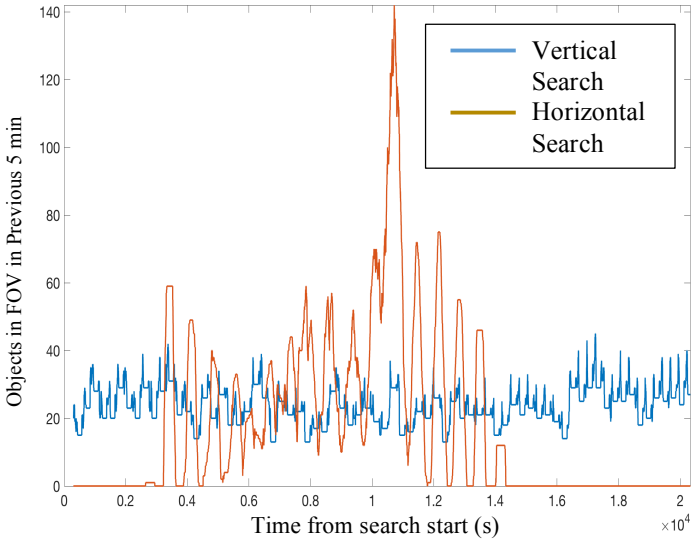

Figure 8: Objects in FOV in previous 5 min for Maui TDI Search

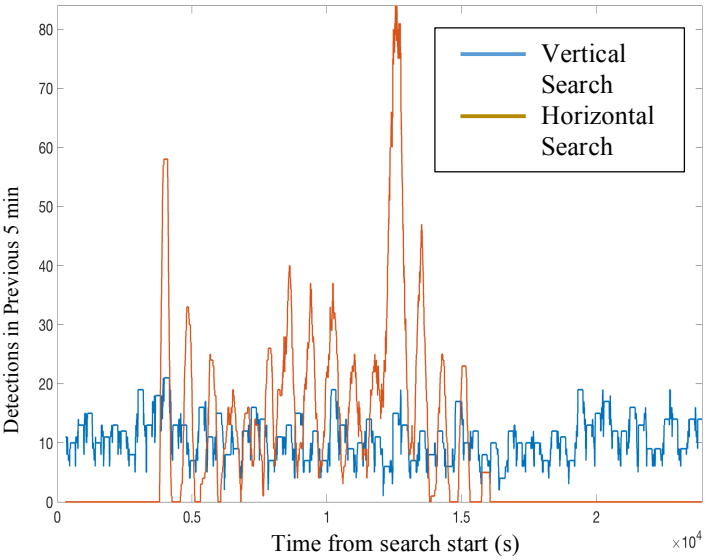

Figure 9: Detections in previous 5 min for Maui Fast Search

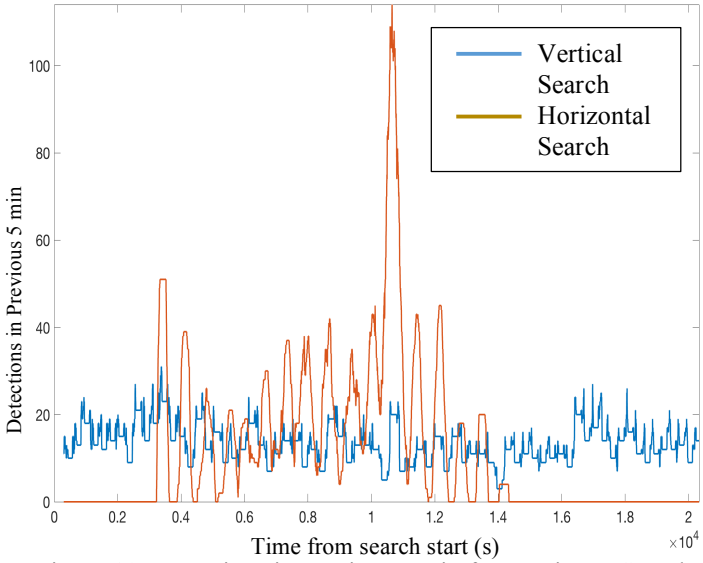

Figure 10: Detections in previous 5 min for Maui TDI Search

Finally, an additional note of interest to any telescope owner/operator is the wear-and-tear on the mount and dome. Over an operational lifespan, the differences in mechanical cycles of a system can play a significant role in the life cycle operating costs for mechanical upkeep and parts replacement. A single cycle is counted each time the mount or dome mechanically starts, moves, and stops during the simulation. While the simulation provides an accurate estimate of mount cycles, the dome cycles require a rough first-order estimate. Dome cycles are entirely dependent on the size, type, and vibrational requirements of the dome and mount. Whereas a clam shell dome may open and close once in the night, a single slit dome on a noisy track may have to rotate and stop before the telescope jitter is sufficiently low to begin taking data. For this estimate, the dome is assumed to be a single slit with a mount azimuth clearance of 20 degrees before causing a vignette on the telescope imagery. As shown in Figure 11, the search pattern and sensor type have a significant impact on the number of mechanical cycles on the mount and dome over a complete search of the 3600 deg^2 search area used in this study.

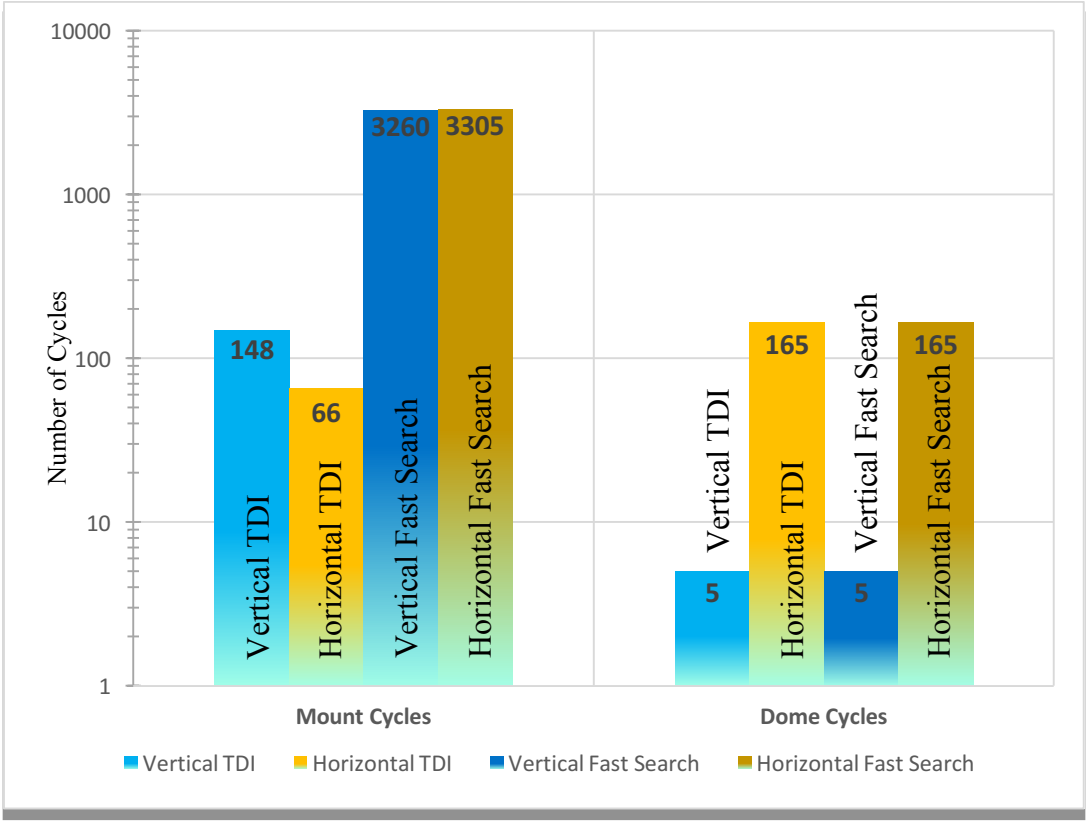

Figure 11: Mount and Dome cycles over single 3600 deg^2 search

Conclusions

While the patterns all perform similarly in the cumulative number of objects detected or discovered in the FOV, slower coverage rates than the 1000 deg^2/hr presented in this simulation using a horizontal search pattern will miss additional high inclination targets. The vertical type searches distribute the detections nearly linearly throughout the search as opposed to the high density of detections in the horizontal searches which may have a significant impact for orbit building. If a wide area search system can leverage a complete and current catalog for correlating detections, then the density of detections may not be as important as other factors such as mechanical usage of the mount, for which the horizontal TDI search pattern has an advantage. This paper also presents a tradeoff between coverage rate and sensitivity which is arguably the most important consideration in implementing a wide area search system, and demonstrates an advantage in implementing a TDI type search at high coverage rates without sacrificing sensitivity. The 1000 deg^2/hr coverage rate presented in this study is relatively high, completing the entire search region in 5 hrs and 40 min (due to the projection of the telescope's perspective on the geostationary belt). The advantage of TDI diminishes at lower coverage rates, and increases at higher coverage rates. GEODSS serves as a useful model to baseline potential performance not only because of its coverage and long history, but because it demonstrates that the wide area search mission can be accomplished with small aperture COTS equipment. It is important to note that this comparison used the same set of notional camera parameters when comparing the Fast Search and TDI scan. Improvements in CCD technology means that sensors can achieve dimmer sensitivities at similar or faster coverage rates than presented in this study, but when comparing to a step-and-stare type search strategy, a TDI scan will maintain an advantage at high coverage rates.

References

[1] Robert F. Bruck, Robert H. Copely. "GEODSS Present Configuration and Potential," Proc. AMOS Tech. Conf (2014)

[2] Ryan D. Coder, Marcus J. Holzinger, "Multi-objective design of optical systems for space situational awareness," Acta Astronautica journal 128, 669-684 (2016)

[3] Choi, Jin et. al. "A Study on the Strategies of the Positioning of a Satellite on Observed Images by the Astronomical Telescope and the Observation and Initial Orbit Determination of Unidentified Space Objects," Journal of Astronomy and Space Sciences. Vol. 28, no. 4, 333-344 (2011)

[4] Paul V. Anderson, "Operational Considerations of GEO Debris Synchronization Dynamics," 66th International Astronautical Congress, IAC-15,A6,7,3,x27478 (2015)